# Ligand Binding to Copper Nanocrystals; Amines, Carboxylic Acids and the Role of Surface Oxides

Arnau Oliva-Puigdomènech,[†,‡] Jonathan De Roo,[†,¶] Jakob Kuhs,[†,§] Christophe Detavernier,[§] Jose C. Martins,[‖] and Zeger Hens[*,†,⊥]

†*Physics and Chemistry of Nanostructures, Ghent University, B9000 Gent, Belgium*

‡*SIM vzw, Technologiepark 935, B9052 Gent, Belgium*

¶*Sol-gel Centre for Research on Inorganic Powders and Thin films Synthesis, Ghent University, B9000 Gent, Belgium*

§*Department of Solid-State Sciences, COCOON group, Ghent University, B9000 Gent, Belgium*

‖*NMR and Structural Analysis Unit, Ghent University, B9000 Gent, Belgium*

⊥*Center for Nano and Biophotonics, B9000 Gent University, Belgium*

E-mail: zeger.hens@ugent.be

**Abstract**

Dispersions and inks based on copper nanoparticles have raised extensive interest for printed electronics as copper holds the promise of attaining high electric conductivity at low cost. Here, we use the decomposition of copper formate in oleylamine to produce a nanocolloid consisting of $\sim 4$ nm copper nanocrystals, a size that is ideal to study the binding of ligands to nanocopper. Using solution $^1$H NMR spectroscopy, we demonstrate that oleylamine binds to the surface of as-synthesized copper nanocrystals, thus stabilizing the dispersion by steric hindrance. We find that addition of a carboxylic acid to a purified nanocolloid induces an exchange between the originally

bound oleylamine and the carboxylic acid as the surface-bound ligand. We provide evidence that the carboxylic acid dissociates upon binding to the copper nanocrystals. As such a process requires an amphoteric surface, a characteristic of a metal oxide but not of an elementary metal, we argue that ligand binding is determined by residual surface oxides and not by the pristine copper surface. Finally, we demonstrate that stable copper nanocolloids can be obtained in a variety of polar solvents by replacing oleylamine as a ligand by 2-[2-(2-methoxyethoxy)ethoxy]acetic acid (MEEAA). The inevitable oxidation of the small copper nanocrystals used here can be undone by mild thermal annealing, which leads especiaaly in the case of MEEAA stabilized nanocopper to significant grain growth. In this way, we turn an as-synthesized dispersion of colloidal copper nanocrystals into a nano-ink that can be formulated to produce metallic copper strips by screen or inkjet printing.

# 1 Introduction

Copper-based nanoparticles have attracted increasing research interest because of their broad application potential, which includes, for example, sensing,[1] heat transfer,[2] light emission,[3,4] surface-enhanced Raman scattering,[5,6] catalysis,[7] and electronics.[8,9] More specifically, in the case of printed electronics, dispersions or inks based on Cu nanocrystals (NCs) can be a cost-effective alternative for Ag-based inks since metallic copper has almost the same bulk conductivity as silver, but is far more abundant.[10] As compared to silver, however, copper is intrinsically prone to oxidation; a problem that becomes particularly relevant when working with Cu NCs. A simple extrapolation of typical oxidation rates of bulk copper, even if they amount to a mere one micrometer *per annum*,[11] indicates that nanometer-sized Cu crystallites can be expected to oxidize completely within a few hours or days.

In the case of Cu NC dispersions or inks, a most interesting approach to suppress or control oxidation involves capping Cu NCs by surface-bound ligands.[10] Exploring the synthesis of nanocrystals in supercritical water, for example, Ziegler and coworkers showed that

hexanethiol, a well known ligand for metal nanocrystals, made copper nitrate react to form Cu instead of CuO nanocrystals, an observation these authors attributed to the formation of a hexanethiol capping at the NC surface.[12] A similar conclusion followed from the work of Kanninen *et al.*[13] who studied the oxidation of Cu NCs capped by aliphatic carboxylic acids and thiols and found that the oxidation rate differed depending on the type of ligand, and the length of the aliphatic chain. Glaria *et al.*[14] analyzed Cu NCs synthesized in the presence of either alkyl amines or phosphonic acids, and showed that stabilization by alkylamines lead to a marked reduction of the oxidation rate. Shi and co-workers,[15] on the other hand, synthesized Cu NCs capped with mercaptocarboxylic acids and studied the reactive oxygen species generated during the oxidation process to assess the cytotoxicity related to this process. In line with the aformentioned studies, these authors found that a longer ligand length prevented the formation of oxygen radicals that lead to cell damage; an indirect indication of the suppression of Cu oxidation.

An important step towards designing a surface termination that protects Cu NCs from oxidizing is understanding how ligands bind and pack on the surface of Cu NCs. This is by no means straightforward. Even in the case of bulk Cu, the mechanism of corrosion protection of a well-known inhibitor such as benzotriazole remains poorly understood.[16] In this respect, Cu NCs can be interesting model systems. Several methods have been developed to analyze the binding of ligands to NCs, such as thermogravimetry, infrared spectroscopy, mass spectrometry or nuclear magnetic resonance (NMR) spectroscopy.[17] Among these different methods to study the surface chemistry of NCs, solution NMR spectroscopy stands out due to its unique capability to identify and quantify NC ligands, and study ligand exchange reactions *in-situ*.[18] In the case of Cu NCs, a few studies have already used solution NMR spectroscopy to investigate ligand binding. Dong and coworkers showed $^{1}$H and $^{13}$C NMR spectra of Cu NCs synthesized in the presence of octanethiol and took the broadening of the resonances as evidence for the formation of a thiol-terminated surface. On the other hand, Glaria *et al.* reported that the synthesis of Cu NCs in the presence of hexadecylamine

leads to surface-bound hexadecylamine that features excessively broadened $^1$H resonances.[14] However, while showing that NMR spectroscopy is instrumental to investigate Cu NCs, these studies did not provide quantitative data on surface coverage or ligand exchange processes. Since such information is essential to understand the ligand binding motif,[19] and accordingly tune the physicochemical properties of Cu NCs, more in depth studies on ligand binding to Cu NCs are needed.

Here, we address the binding of amines and carboxylic acids to Cu NCs, two commonly used ligands in NC research, by combining solution NMR spectroscopy with judicious ligand exchange experiments. As a study object, we use $\sim$ 4 nm Cu NCs synthesized by the decomposition of Cu formate in the presence of oleylamine. We show that the crude reaction product can be purified by means of standard purification protocols to obtain dispersions that contain, next to the solvent and the Cu NCs, almost exclusively surface-bound ligands. Using a set of 1D and 2D $^1$H NMR techniques,[18] we demonstrate that oleylamine is a tightly bound ligand and we estimate a sample-dependent surface concentration in the range $1.4-2.5\,\mathrm{nm}^{-2}$. A most remarkable finding is that addition of undecenoic acid to oleylamine-stabilized Cu NCs results in the nearly 1 equivalent exchange at the Cu surface, which again results in a tightly-bound ligand shell. Importantly, this surface reaction results in the binding of a dissociated acid on the Cu surface, a reaction similar to what was described by De Roo *et al.* in the case of metal oxide nanocrystals.[20] We therefore propose that ligands such as amines and carboxylic acids mostly interact with Cu NCs through surface bound copper oxide. Based on these findings, we show that a similar ligand exchange reaction enables Cu NCs to be functionalized with 2-[2-(2-methoxyethoxy)ethoxy]acetic acid,[21] an approach that stabilizes Cu nanocolloids in the polar solvents typically used in printed electronics. Moreover, while air exposure induces a rapid oxidation of the small Cu NCs used here, reduced copper can be readily obtained by mild thermal annealing of a NC film, where the use of the more volatile MEEAA ligands significantly promotes sintering.

## 2 Experimental Section

**Chemicals.** In this work, the following chemicals were used: copper(II) formate tetrahydrate (Alfa Aesar, 98%), bicinchoninic acid disodium salt hydrate (Sigma-Aldrich ≤98%), oleylamine (Acros Tech, 80-90%), n-dodecane (Merck Millipore, ≤99%), acetonitrile (VWR, ≤99.5%), n-hexane (VWR, 98%), methanol (VWR, ≤99.8%), undecenoic acid (Sigma-Aldrich, 98%), 2-[2-(2-methoxyethoxy)ethoxy]acetic acid (Sigma-Aldrich, technical grade), deuterated toluene (Sigma-Aldrich, ≤99.6%). All the solvents utilized during synthesis and purification were degassed prior to use by freeze-thawing method to remove dissolved oxygen.

**Synthesis of copper nanocrystals.** Copper nanocrystals were synthesized by an adaptation of the method originally introduced by Sun *et al.*[22] In brief, a solution of copper(II) formate tetrahydrate (0.2 mol/L) in an 20 mL oleylamine:dodecane mixture (1:1 by volume) was formed by heating the mixture at 60 °C until the copper(II) formate was fully dissolved. Next, the solution was held at 60 °C under vacuum for 1 hour to remove excess water. Upon raising the temperature to 140 °C, the color of the reaction mixture changed from blue to dark red, indicating the reduction of copper(II) to metallic copper. This reaction mixture was kept at 140°C for 5 minutes, cooled down and diluted with hexane to prevent nanocrystal aggregation. Finally, the resulting solution was washed multiple times using acetonitrile and methanol as non-solvents and hexane as a solvent.

**Quantification of $Cu^+$ and $Cu^0$.** The amount of $Cu^+$ and $Cu^0$ was quantified by taking aliquots from the reaction mixture at different stages of the reaction. For the quantitative analysis of $Cu^+$, these aliquots were weighted, diluted in hexane and loaded in a small glass vial. Right after, a known concentration of bicinchoninic acid dissolved in DMSO was added to the vial, which resulted in a 2-phase system. Upon shaking, the $Cu^+$ could be extracted from the reaction mixture, and an intensely colored $Cu^+$ complex with bicinchoninic acid was formed in the DMSO phase. Subsequently, the amount of $Cu^+$ was determined col-

orimetrically, from the absorbance of the DMSO phase at 562 nm using a molar extinction coefficient of $7.7\,10^3$l/(mol $\cdot$ cm).[23] For the quantification of $Cu^0$, the aliquots were diluted in hexane and the absorbance spectra of the resulting dispersion was directly recorded. The intrinsic absorption coefficient of $Cu^0$ at 400 nm in hexane was calculated using its optical constants: $n = 1.32, k = 2.12$.[24] From the combination of the intrinsic absorption coefficient and the absorbance of the Cu NC dispersions at 400 nm, the volume fraction of Cu in the dispersion was obtained, a number that directly yields the amount of $Cu^0$ formed in the reaction.[25]

**NMR analysis.** Samples for NMR analysis were prepared by drying the purified reaction product under a nitrogen flow and redispersing the resulting powder in toluene-$d_8$. To prevent oxidation, all purification and sample preparation was performed under an inert atmosphere in a nitrogen-filled glovebox and the samples were loaded in air-tight screw-capped NMR tubes. NMR spectra were recorded either on a Bruker Avance III Ascend Spectrometer operating at a $^1$H frequency of 500.13 MHz and equipped with a BBI-Z probe or on a Bruker Avance II Spectrometer operating at a $^1$H frequency of 500.13 MHz and equipped with a TXI-Z probe. The sample temperature was set at 298.15 K. Quantitative $^1$H spectra were recorded with 20 s delay between scans to ensure full relaxation of all NMR signals and concentrations were determined using the Digital ERETIC method. Diffusion-Ordered Spectroscopy (DOSY) experiments were performed using a double stimulated echo sequence for convection compensation and with monopolar gradient pulses. The diffusion decay was recorded in 64 steps of squared gradient strength from 95% to 2% of the probe's maximum value. The gradient pulse duration and diffusion delay were optimized so as to guarantee at least a 10-fold attenuation of the signal throughout the gradient strength scan.

**Structural Characterization.** Transmission electron microscopy (TEM) images were recorded on a Cs-corrected JEOL 2200-FS TEM operated at 200 kV. FTIR samples were prepared under inert atmosphere by dispersing a solution of Cu NCs in tetrachloroethy-

lene and measuring them inside a KBr coated cuvette using a Nicolet 6700 FTIR. UV/Vis measurements were performed using an Avantes Ava-Spec-2048 spectrometer using Avantes Avalight-DH-S-BAL as a light source.

**Ligand Surface Concentration.** The surface concentration of bound ligands was estimated by combining (1) the overall concentration of bound ligands as determined using NMR spectroscopy (see paragraph on NMR analysis), (2) the average surface area of the Cu NCs as determined using TEM imaging, and (3) the concentration of Cu NCs in the dispersion. For the latter, we used spectrophotometry to determine the total amount of Cu in the dispersion (see paragraph on quantification of $Cu^+$ and $Cu^0$) and TEM to determine the average NC volume. The ligand surface concentration is then obtained as the ratio between the number of ligands in the dispersion and the total area of the Cu NCs in the dispersion.

**Ligand Exchange to UDA.** In an oxygen-free environment, excess UDA (5-fold to $OlNH_2$) was added to a dispersion of $OlNH_2$ capped Cu NCs in hexane. After keeping the dispersion at room temperature for 30 minutes, the Cu NCs were precipitated by addition of acetonitrile and methanol as non-solvents and the thus obtained Cu NC powder was redispersed in hexane. This process was repeated a second time, followed by multiple purification cycles.

**Ligand Exchange to MEEAA.** In an oxygen-free environment, an hexane solution of $OlNH_2$ capped Cu NCs was dried under $N_2$ flow. After, 2-[2-(2-methoxyethoxy)ethoxy]acetic acid (MEEAA) and methanol were added and the solution was left under stirring until the NCs were fully dispersed in the methanol solution. The resulting solution of MEEAA capped NCs was washed of excess MEEAA and released $OlNH_2$ using a combination of methanol, isopropanol and hexane where the first and second act as solvents and the last as non-solvent.

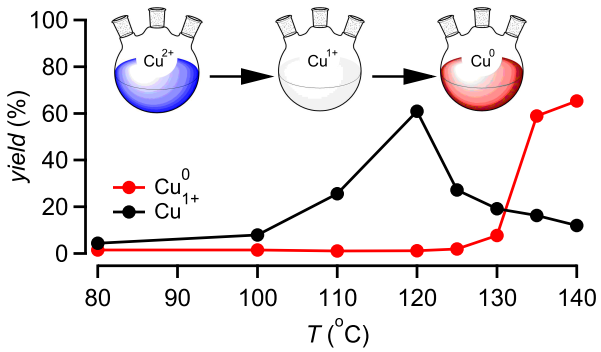


Figure 1: Development of the yield of (black) $Cu^{1+}$ and (red) $Cu^0$ during a typical Cu NC synthesis based on heating a copper formate solution in an 1:1 oleylamine:dodecane mixture up to 140 °C. All datapoints at intermediate temperatures were obtained by analyzing aliquots taken from the reaction mixture during the temperature sweep. In the case of the datapoint at 140 °C, the reaction was kept at that final temperature for 5 minutes before the aliquot was taken.

***In-situ* XRD.** *In-situ* X-ray diffraction (XRD) was used to monitor the sintering of the Cu nanocrystals as a function of temperature. While linearly increasing the temperature of the sample in a controlled ambient, XRD patterns were obtained using a Bruker D8 Discover equipped with a Cu K$\alpha$ x-ray source and a linear detector. The series of diffractograms were plotted as a function of temperature and diffraction angle using a color-scale map for the recorded intensities, where red represents a higher intensity.

# 3 Results

## 3.1 Copper Nanocrystals, Synthesis and Characterization

Copper NCs were synthesized by the thermal decomposition of copper formate ($Cu(HCO_2)_2$) in a mixture of dodecane and oleylamine ($OlNH_2$), an approach inspired by the method proposed by Sun *et al.*[22] In practice, a 0.2 M solution of $Cu(HCO_2)_2$ in a 1:1 mixture of $OlNH_2$ and dodecane was heated to 140 °C and kept at that temperature for 5 minutes. Upon heating at a rate of approximately 10 °C/min, the deep blue color of the initial solution first became transparent at around 120 °C, after which the reaction mixture quickly turned dark

red; a color typical of dispersions of Cu NCs. We hypothesized that these color changes reflect the successive reduction of $Cu^{2+}$ into $Cu^{1+}$ and, finally, metallic $Cu^0$. To confirm this, we quantified the amount of $Cu^{1+}$ and $Cu^0$ in the reaction mixture at different stages of the reaction using colorimetry, where we quantified $Cu^{1+}$ through selective complexation with bicinchoninic acid, and $Cu^0$ by means of the absorption coefficient of metallic Cu NCs (see Experimental Section). Figure 1 represents the composition of the reaction mixture obtained in this way. In line with our hypothesis, metallic Cu is indeed formed in a two-step process. The initially present $Cu^{2+}$ is first reduced at temperatures between 100 and 120 °C to form $Cu^{1+}$, which only gives way to metallic copper at temperatures above 130 °C. When keeping the reaction mixture at 140 °C for 5 minutes, we estimate that ∼65% of the $Cu^{2+}$ originally present is converted into metallic Cu. Such a yield is similar to what was reported by Sun *et al.*,[22] yet the reaction is carried out at only 140 °C during 5 minutes instead of 250 °C for 20 minutes.

Figure 2a represents a typical bright field transmission electron microscopy (TEM) image of the reaction product obtained from the decomposition of $Cu(HCO_2)_2$. As can be seen, the synthesis method resulted in quasi-spherical particles with an average diameter of $3.95 \pm 0.04$ nm and a size dispersion of $\sim 20\%$. According to the selected area electron diffraction (SAED) pattern shown in Figure 2b, the particles are crystalline and feature lattice spacings characteristic of metallic Cu. The formation of Cu NCs is further confirmed by the UV-Vis spectra of the purified reaction product (in red), which feature the absorbance maximum at 560 nm that is characteristic of the surface plasmon resonance (SPR) of spherical Cu NCs (see Figure 2c).[26] In line with previous studies,[13,14] exposing the Cu NCs to air resulted in a gradual redshift of the SPR, which reached 605 nm after 120 seconds of permanent air exposure for the example shown in Figure 2c. Further air exposure resulted in the complete disappearance of the SPR. Such a variation of the absorbance spectrum is typically attributed to the progressive oxidation of the Cu NCs, an interpretation we confirmed by means of an SAED analysis of the NCs after air exposure. As can be seen in Figure 2d, the SAED

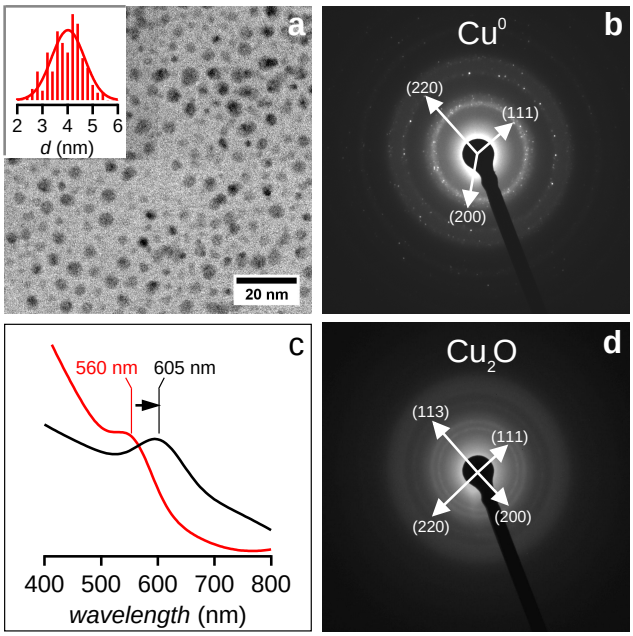


Figure 2: (a) Low-resolution, brightfield TEM image of a typical synthesis of Cu NCs; (inset) Size histogram determined based on the analysis of 300 NCs in TEM images. (b) Selected Area Electron Diffraction (SAED) pattern of a sample of pristine (i.e., no air exposure) Cu NCs. (c) UV-Vis spectra of a sample of Cu NCs, (red) pristine, (black) after 120 seconds of air exposure. Spectra have been normalized at the maximum intensity of the plasmon resonance. (d) Selected Area Electron Diffraction (SAED) pattern of a Cu NCs sample exposed to air for 5 days.

patterns of a sample exposed to air for 5 days indeed features four diffraction rings that can be assigned to diffraction from the (111), (200), (220) and (113) lattice planes of $Cu_2O$, corroborating the conclusion that the 3 nm copper NCs studied here rapidly oxidize when exposed to air.

## 3.2 Surface Chemistry of As-Synthesized Cu Nanocrystals

Figure 3a shows a 1D $^1$H NMR spectrum recorded on a purified dispersion of Cu NCs in toluene-$d_8$, synthesized as described above. As the Cu NCs studied here are prone to oxidation, air exposure was avoided during all stages of the synthesis, sample preparation and analysis. In practice, this means that all work was carried out in a nitrogen-filled glovebox, until samples were loaded in air-tight NMR tubes. Next to the narrow resonances of residual

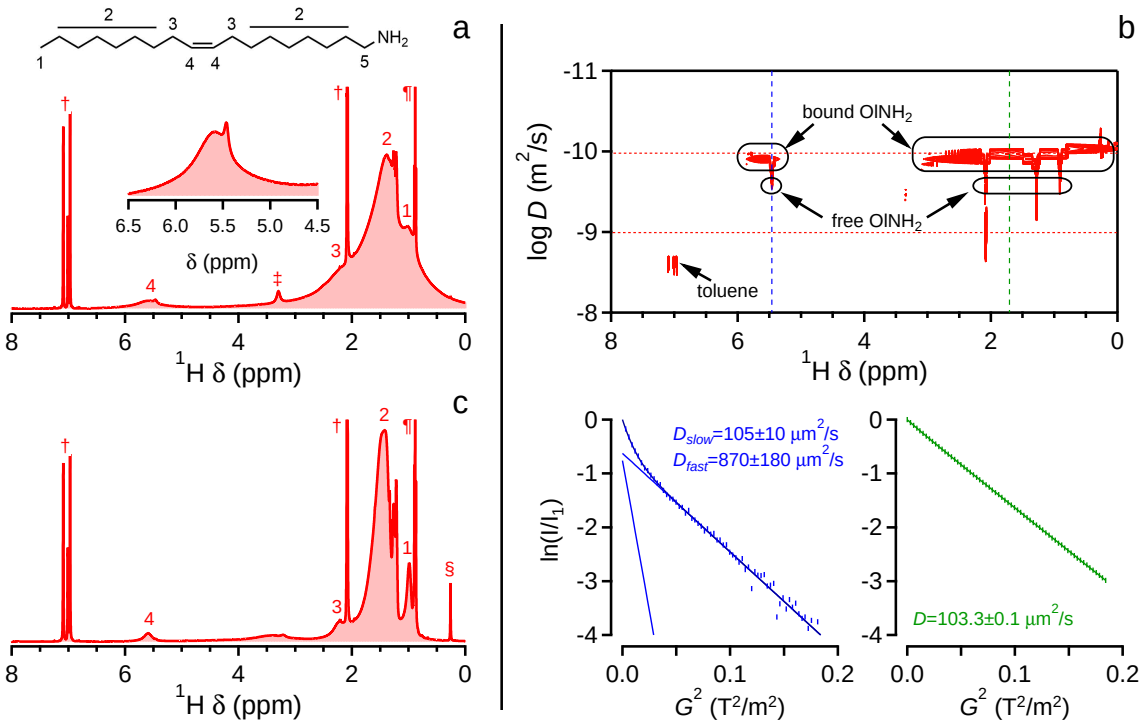


Figure 3: (a) 1D $^1$H NMR spectrum of Cu NCs capped with $OlNH_2$ in toluene-$d_8$. (b) (top) DOSY NMR spectrum of the same Cu NC dispersion and (bottom) decay of the signal intensity as a function of the square of the field gradient strength as obtained at chemical shifts as indicated in the DOSY spectrum. (c) 1D $^1$H NMR spectrum of Cu NCs capped with $OlNH_2$ after air exposure. Labeled resonances are identified as (1-5) $OlNH_2$ resonances, (‡) residual methanol, (¶) hexane, (†) toluene-$d_8$ and (§) silicon grease.

toluene at around 7.0 and 2.1 ppm, the spectrum is dominated by broad resonances that are assigned to the different protons in the oleyl chain, as indicated. The resonance of the alkene protons **4** is retrieved at around 5.5 ppm, whereas most of the methyl protons **2** contribute to the broad resonance that peaks at around 1.5 ppm and the methyl protons **1** yield a minor shoulder at 1.0 ppm. Line broadening reduces the resonance of the protons **3** to a slight shoulder at around 2.2 ppm and makes that the resonance of the $\alpha$-proton **5** cannot be discerned at all. In addition, the spectrum features resonances of methanol and hexane, which were used as non-solvent and solvent in the purification process. For a more detailed account of the resonance assignment, see Supporting Information S1.

Figure 3b represents the DOSY spectrum of the same sample, which shows that the broad oleyl resonances are linked to species with a diffusion coefficient that is markedly smaller

Table 1: Full width at half maximum of 3 selected resonances of the oleyl chain as measured on dispersions of as-synthesized and oxidized Cu NCs, and a dispersion of CdSe NCs in toluene-$d_8$.

| Resonance | Cu as-synthesized | Cu oxidized | CdSe as-synthesized |
|---|---|---|---|
| 2 | 400 Hz | 145 Hz | 140 Hz |
| 4 | 235 Hz | 85 Hz | 75 Hz |
| 1 | NA | 50 Hz | 42.5 Hz |

than the self-diffusion coefficient of toluene. A detailed analysis of the signal intensity as a function of the field gradient strength at around 1.7 ppm – a chemical shift where only the broad $OlNH_2$ resonance is observed – yields a diffusion coefficient of $103.3 \pm 0.1\,\mu m^2/s$ (see Figure 3b). In toluene, such a diffusion coefficient corresponds to a solvodynamic diameter of $7.16 \pm 0.01$nm. Since this number corresponds to the sum of the NC diameter (4.0 nm) and twice the estimated length of an oleyl chain ($1.5 - 2.0$ nm), we conclude that in the case of Cu NCs, $OlNH_2$ acts as a tightly bound ligand.

As shown in the inset of Figure 3a, the signal of the alkene protons feature next to the broad resonance of bound $OlNH_2$ a more narrow resonance. According to the DOSY spectrum, this latter resonance comes with a larger diffusion coefficient than bound $OlNH_2$. This point can be clearly seen in the decay of the resonance intensity with increasing field gradient strength as shown in Figure 3b. As shown in the bottom section of Figure 3b, fitting the intensity decay to a bi-exponential, yields a diffusion coefficient of the slow and the fast component of $105 \pm 10\,\mu m^2/s$ and $870 \pm 180\,\mu m^2/s$. Since the latter value is only slightly smaller than the diffusion coefficient of $OlNH_2$ in toluene ($1022 \pm 4\,\mu m^2/s$), we conclude that this resonance pertains to free $OlNH_2$ in the Cu NC dispersion.

The most striking feature of the spectrum shown in Figure 3a is the excessive broadening of the oleyl resonances, in line with the previous study of Glaria *et al.*[14] As shown in Table 1, the alkene proton resonance **2** at 5.58 ppm has a full width at half maximum of 235 Hz, whereas the bulk methylene resonance **1** and the methyl resonance **3** yield one broad resonance that is 400 Hz wide. These numbers are about 3 times larger than the corresponding

resonances in the case of semiconductor NCs, such as CdSe (see Supporting Information S2). Possibly, this line broadening results from a different magnetic environment experienced by $OlNH_2$ when bound to Cu NCs, in agreement with previous reports on paramagnetism in Cu NCs.[27]

Despite the pronounced line broadening, the alkene proton resonance **4** remains well resolved, and based on its integrated intensity, we estimated that the sample analyzed here has a surface concentration of bound $OlNH_2$ of $1.4\,nm^{-2}$. As compared to semiconductor NCs, which often have ligand surface concentrations in the range $3.0-5.0\,nm^{-2}$, this number is rather low. Possibly, this is due to the significant line broadening, which can make that the resonance intensity is partially lost in the background noise. On the other hand, such surface concentrations are not unrealistic, since they suffice to preserve colloidal stability.[17]

Figure 3c displays the $^1H$ NMR spectrum of a dispersion of Cu NCs in toluene-$d_8$ that was opened to air after sample preparation. As compared to the spectrum shown in Figure 3a, one sees that oxidation results in a significant narrowing of the resonances of bound $OlNH_2$, which now feature line widths comparable to what is typically recorded for semiconductor NCs (see Table 1). Importantly, as shown in the Supporting Information S3, oxidation does not affect the diffusion coefficient of the $OlNH_2$ resonances, *i.e.*, $OlNH_2$ remains a tightly bound ligand. This suggests that the narrowing of the $OlNH_2$ resonances upon oxidation is not caused by bound $OlNH_2$ assuming a different physical state. However, it may reflect the loss of the specific magnetic environment of Cu NCs upon oxidation, with the resulting $Cu_2O$ NCs being a diamagnetic material similar to the CdSe NCs we used as a reference in Table 1.

Among the signals assigned to methanol and hexane, the behavior of the methanol (MeOH) resonance stands out. The resonance is broadened and shifted from its expected position, which suggests that it interacts with the NC surface. Support for this hypothesis comes from the DOSY spectrum, where the MeOH resonance comes with a diffusion coefficient of $166 \pm 18\,\mu m^2/s$. That changes after oxidation of the particles, which results

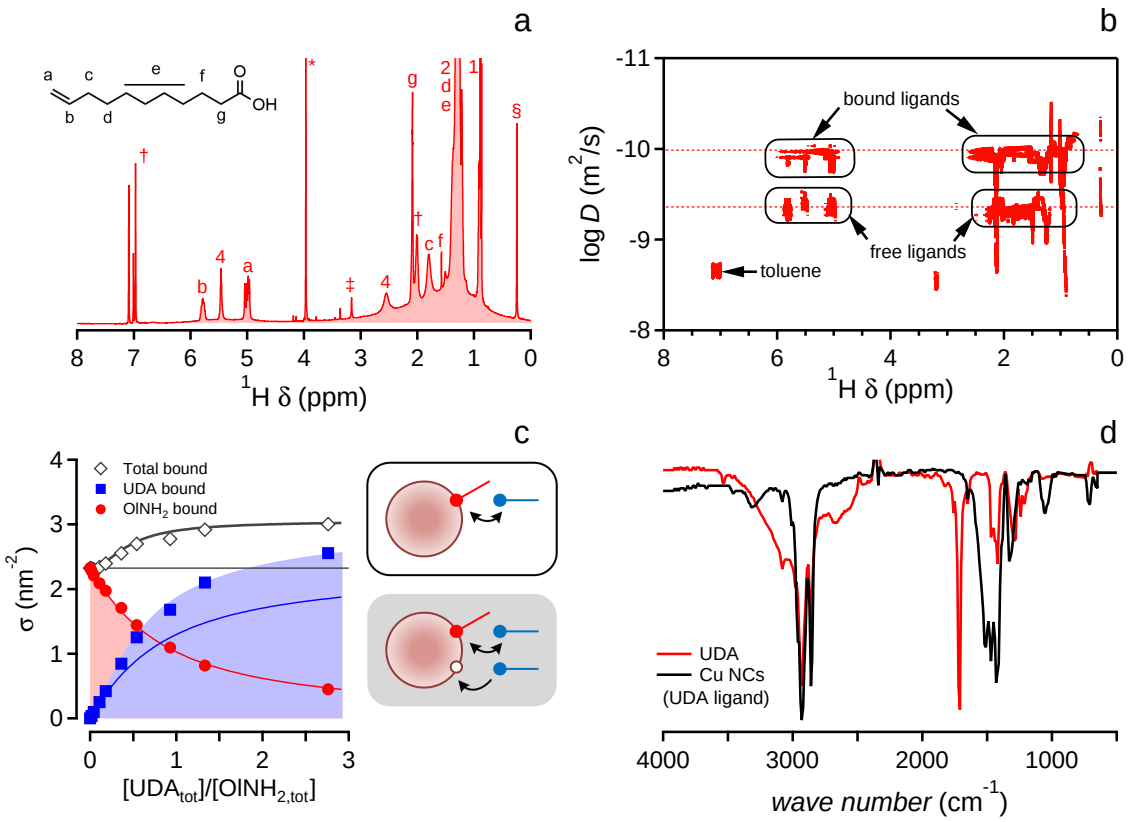


Figure 4: (a) 1D $^1$H NMR spectrum of Cu NCs after addition of UDA in toluene-$d_8$. (b) DOSY NMR spectrum of the same Cu NCs dispersion. (c) Evolution of the bound ligands in the surface of Cu NCs during the progressive addition of UDA on $OlNH_2$ capped NCs. (d) Solution FTIR spectra of UDA (red) and Cu NCs after addition of UDA (black). Labeled resonances are identified as (a-g) UDA signals, (1-5) $OlNH_2$ signals, (*) dibromomethane, (§) residual grease, (‡) methanol and (†) toluene-$d_8$.

in a marked increase of the diffusion coefficient, up to a value of $D = 1046 \pm 145\ \mu m^2/s$. As this number remains well below the diffusion coefficient of MeOH in toluene, which was determined at $2834 \pm 41\ \mu m^2/s$, this indicates that the MeOH still interacts, albeit more weakly, with oxidized Cu NCs.

## 3.3 Carboxylic Acids as Ligands for Cu Nanocrystals

To have more versatility to design the ligand shell of Cu NCs, we analyzed the exchange of the originally present $OlNH_2$ ligands for carboxylic acids, a class of ligands widely used with semiconductor and metal oxide NCs. To monitor the possible exchange of $OlNH_2$

for carboxylic acids, we used undecenoic acid (UDA) as the carboxylic acid of choice since it features two distinct alkene resonances that show little overlap with the resonances of $OlNH_2$ (see Supporting Information S4). As shown in Figure 4a, addition of UDA gave rise to several new signals in the $^1$H NMR spectrum of as-synthesized Cu NCs. The multiple narrow resonances in the aliphatic region can be attributed to protons of both UDA and $OlNH_2$, as indicated. Interestingly, upon adding the carboxylic acid, the appearance of the alkene resonance of $OlNH_2$ at 5.58 ppm changed dramatically. The initially broad resonance has been mostly replaced by a narrow resonance at 5.47 ppm. Such a change points towards the release of the bound $OlNH_2$ from the Cu surface. Finally, the characteristic alkene resonances of UDA show up as narrow signals 4.98 and 5.78 ppm on top of a broad background feature. The DOSY spectrum shown in Figure 4b confirms that the signals of the alkene resonances of both UDA and $OlNH_2$ come with two distinct diffusion coefficients; a small diffusion coefficient characteristic of surface-bound ligands, and a larger diffusion coefficent that is consistent with a pool of free ligands. Interestingly, also the diffusion coefficient of MeOH markedly increases after UDA addition, up to a value characteristic of free MeOH. We thus conclude that addition of a carboxylic acid such as UDA induces the release $OlNH_2$ from the Cu NC surface and suppresses the interaction of MeOH with this surface.

To evaluate in more detail the relation between UDA addition and $OlNH_2$ release, we titrated a purified dispersion of as-synthesized, $OlNH_2$-capped Cu NCs with UDA. As shown in Figure 4c, we started in this case with Cu NCs having a bound $OlNH_2$ surface concentration $\sigma_{OlNH_2}$ of 2.3 $nm^{-2}$, and added up to 3 equiv of UDA, relative to the initial $OlNH_2$ concentration. It can be seen from Figure 4c that in the initial stages of the titration, UDA exchanges almost quantitatively for $OlNH_2$. Further increasing the amount of UDA in the dispersion leads to a progressive enrichment of the ligand shell in bound UDA, yet adding 1 equiv of UDA does not suffice to remove all $OlNH_2$. Nevertheless, it can be seen from Figure 4c that the increase of bound UDA in the ligand shell resembles reasonably well the loss of bound $OlNH_2$ across the entire titration curve.

The correspondence between UDA binding and $OlNH_2$ release suggests that the effect of UDA addition can be described by a simple exchange process where bound UDA forms by removing bound $OlNH_2$, a process sketched in the unfilled box in Figure 4c:

$$(Cu)[OlNH_2] + UDA \rightleftharpoons (Cu)[UDA] + OlNH_2 \quad (1)$$

By means of the equilibrium expression of this exchange reaction, the concentration of either of the bound ligands can be obtained as a function of the total concentration of UDA in the dispersion, see Supporting Information S5. The full lines included in Figure 4c represent a simulation of the $OlNH_2$/UDA exchange according to the equilibrium reaction 1. As can be seen, the approach leads to a good description of the $OlNH_2$ coverage, and it predicts the initial quantitative replacement of $OlNH_2$ by UDA. In fact, the quantitative replacement of $OlNH_2$ by UDA at low UDA concentrations is a distinctive characteristic of the equilibrium reaction 1, see Supporting Information S5.

An immediate consequence of the one-for-one ligand exchange as described by reaction 1 is that the total surface concentration $\sigma_{tot}$ of ligands remains constant. This is not the case for the exchange reaction studied here. While the first UDA additions have little effect on $\sigma_{tot}$, Figure 4c shows that adding more UDA increases $\sigma_{tot}$ from 2.3 to 3.0 $nm^{-2}$; an evolution that is not described by the model simulation based on Eq 1. The increased surface coverage indicates that, next to replacing $OlNH_2$, UDA can also bind to Cu NCs by occupying additional, originally unoccupied surface sites, a process depicted in the filled box added to Figure 4c:

$$(Cu)[\circ] + UDA \rightleftharpoons (Cu)[UDA] \quad (2)$$

This reaction can be seen in two different ways, which differ in terms of the affinity of these empty surface sites for binding $OlNH_2$. As outlined in Supporting Information S6, a model where the additional binding sites can bind both ligands fails to describe the initial quantitative replacement of bound $OlNH_2$ by the added UDA. On the other hand, a satisfactory

description of the experimental $OlNH_2$/UDA titration is obtained under the assumption that these unoccupied sites have little affinity for binding $OlNH_2$, see Supporting Information S7. The resulting simulation of the $OlNH_2$/UDA titration is represented by the filled areas in Figure 4c. We thus conclude that the addition of a carboxylic acid such as UDA to $OlNH_2$-capped Cu NCs has two effects; as described by the equilibrium reactions 1 and 2, UDA both exchanges with bound $OlNH_2$ and binds to empty sites at the Cu NC surface. From the equilibrium constants obtained from a best fit of this so-called heterogeneous binding site model to the experimental titration curves, we estimate that the free energy change of the UDA/$OlNH_2$ exchange is a mere $-1.1\,\mathrm{kJ\cdot mol^{-1}}$, whereas the free energy of UDA adsorption amounts to $\sim -30\,\mathrm{kJ\cdot mol^{-1}}$. Note that the increased coverage of binding sites after UDA addition may also account for the observation that UDA addition suppresses the interaction between MeOH and the Cu NC surface.

The exchange between carboxylic acids and amines at NC surfaces was observed before in the case of metal oxide NCs.[20] In that case, this reaction was seen as a property of the specific binding motif of carboxylic acids to metal oxides, which involved the dissociative binding of the carboxylate and the proton to Lewis acidic and basic surface sites, respectively. Keeping that finding in mind, we investigated the binding of UDA to Cu NCs in more detail. Figure 4d represents the IR spectrum of UDA and of a dispersion of Cu NCs passivated with UDA. As expected, the UDA reference spectrum shows the characteristic signatures of the carboxyl group, including the C=O stretch vibration at $1720\,\mathrm{cm^{-1}}$, the in-plane C-O-H bend vibration at $1420\,\mathrm{cm^{-1}}$, and the C-O stretch vibration at $1300\,\mathrm{cm^{-1}}$. In addition, a broad feature ranging from 3500 to $2500\,\mathrm{cm^{-1}}$ can be seen, which can be assigned to the O-H stretch vibration. In the case of the Cu NC dispersion, however, the C=O stretch vibration and the broad feature assigned to the O-H stretch vibration are notably absent. In addition, new features appear at around $1500\,\mathrm{cm^{-1}}$ that are often assigned to both asymmetric and symmetric stretching of a metal-bound carboxylate. Given the requirement that the exchange reaction 1 be charge neutral in apolar media, we thus conclude that UDA

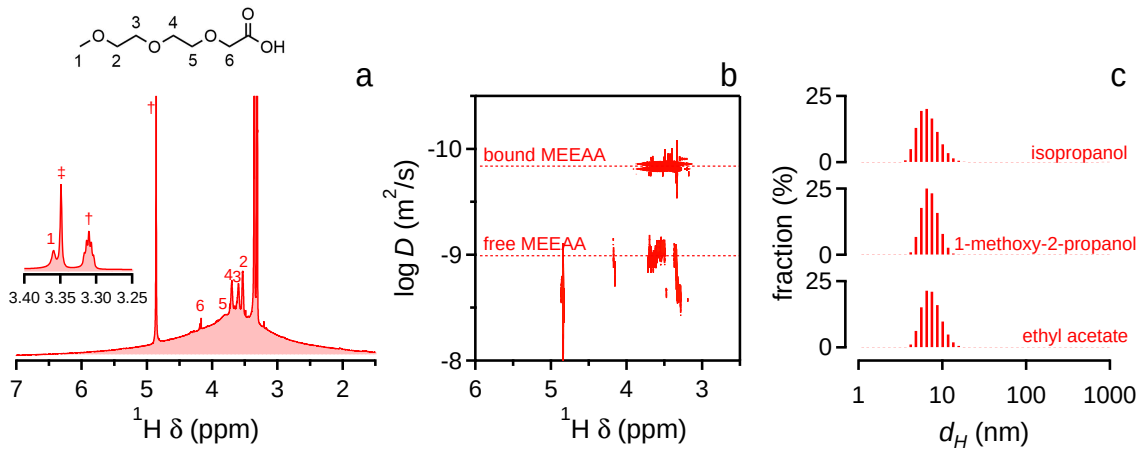


Figure 5: (a) 1D $^1$H NMR of Cu NCs after ligand exchange to MEEAA and dispersed in methanol$_d$4. (b) DOSY spectra of the same Cu NCs dispersion. (c) Hydrodynamic diameter distribution by Dynamic light scattering (DLS) of Cu NCs capped with MEEAA in different solvents. Labeled resonances are identified as (1-6) MEEAA resonances, (‡) methanol and (†) residual methanol-$d_4$.

dissociates upon binding to Cu NCs in a carboxylate and a proton, not unlike the binding motif carboxylic acids feature upon interaction with metal oxide NCs.

## 3.4 Transfer of Cu Nanocrystals to Polar Solvents by Ligand Exchange

Recently, 2-[2-(2-methoxyethoxy)ethoxy]acetic acid (MEEAA) was put forward as a versatile ligand that enables dispersions of semiconductor and metal oxide NCs to be stabilized in a variety of solvents, ranging from toluene to water.[21] The replacement of the original $OlNH_2$ ligands by UDA as demonstrated in the previous section suggests that MEEAA could be an equally versatile ligand for Cu NCs. As outlined in the Experimental Section, we found that a solution of MEEAA in methanol indeed disperses a dry powder of $OlNH_2$-capped Cu NCs; a dispersion that can be purified using hexane as the non-solvent and methanol or isopropanol as the solvent.

Figure 5a-b represents the $^1$H 1D and DOSY spectrum of a dispersion of Cu NCs in methanol-$d_4$ prepared as outlined above. It can be readily seen that no resonances of the

originally present $OlNH_2$ remain in the 1D $^1$H NMR spectrum. Instead, a broad signal ranging from 6 to 1.5 ppm is obtained, together with a few superimposed narrow resonances. The latter could be assigned either to MEEAA, methanol or residual methanol-$d_4$ (see Supporting Information S8). According to DOSY, the narrow resonances have a diffusion coefficient $D = 805 \pm 18\ \mu m^2/s$, which agrees with the diffusion coefficient of MEEAA in methanol. The broad background resonance, on the other hand, features a markedly smaller diffusion coefficient of $139 \pm 1\ \mu m^2/s$, a number corresponding to a hydrodynamic diameter of $5.76 \pm 0.01$ nm in methanol. Since this figure agrees with the expected for MEEAA-capped Cu NCs, we assign the broad resonance to tightly bound MEEAA. Note that also in this case, the resonance is significantly broader than the reported resonances of MEEAA bound to $HfO_2$ or CdSe NCs.[21]

To highlight the versatility of MEEAA as a ligand to stabilize Cu NCs in polar solvents, we assessed the particle distribution of nanocolloids made by dispersing MEEAA-capped Cu NCs in ethyl acetate, isopropanol and 1-methoxy-2-propanol using dynamic light scattering (DLS). Figure 5c represents the particle size distributions as recorded on dispersions of the same batch of Cu NCs in each of these solvents. A monomodal size distribution is obtained in each case, that systematically attains a maximum at around 7 nm. As this solvodynamic diameter agrees with the value determined using DOSY for MEEAA-capped Cu NCs dispersed in methanol, we conclude that in each of these solvents, a MEEAA capping results in stable dispersions of individual Cu NCs. In this respect, it is worth mentioning that MEEAA has a boiling point of a mere 140 °C, as compared to the 360 °C of $OlNH_2$. This suggests that upon annealing films of MEEAA stabilized Cu NCs, dense Cu films can be obtained at a relatively low large temperature.

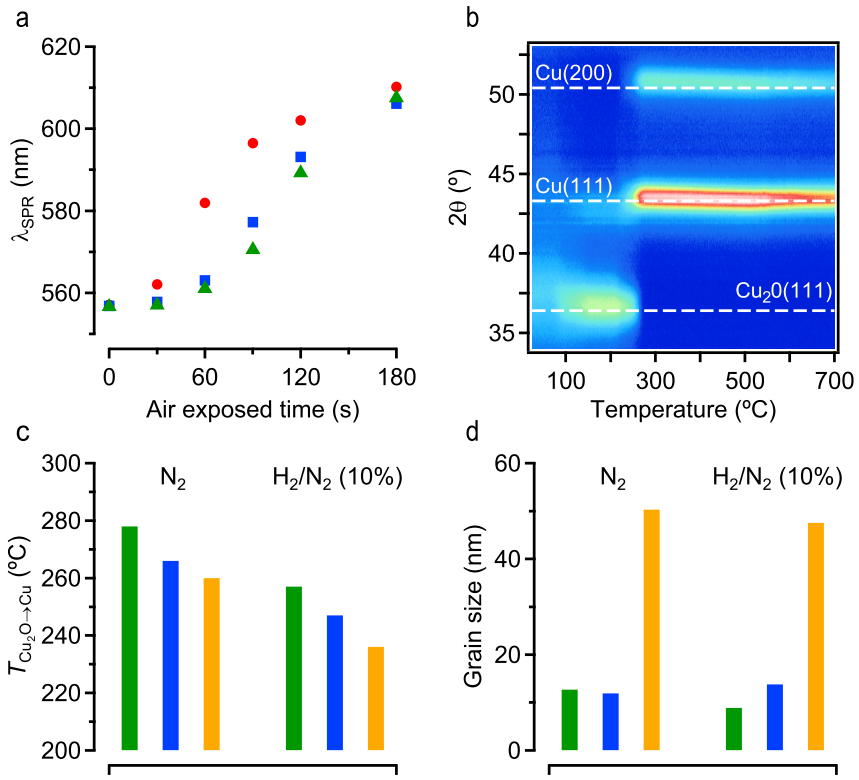


Figure 6: (a) Peak wavelength of the surface plasmon resonance after starting the permanent exposure of a dispersion of Cu NCs to air. The different data sets pertain to Cu NCs capped by (red circles) $OlNH_2$, (blue squares) UDA, and (green triangles) oleic acid. (b) Contour plots of x-ray diffractograms of films of dropcast, UDA-capped Cu NCs recorded *in-situ* during annealing under $N_2$. (c) Transition temperature characterizing the reduction of $Cu_2O$ NCs to Cu, depending on the ligand and the annealing atmosphere. Each bar represents a different ligand: (blue) UDA, (green) oleic acid and (orange) MEEAA. (d) Grain size of the crystallites as obtained from the diffractogram recorded at 300°, depending on the ligand and annealing atmosphere.

## 3.5 Ligand-Dependent Oxidation, Annealing and Sintering of Cu Nanocrystals

Given the interest of Cu NCs for printed electronics, we investigated the impact of the different surface ligands we introduced on the oxidation and sintering behavior of the 4 nm Cu NCs studied here. To assess the oxidation rate, unoxidized Cu NCs capped with different ligands were exposed to ambient conditions, after which we regularly recorded the absorbance spectrum of the dispersion. As shown in Figure 6a, permanent air exposure induces a rapid

redshift of the surface plasmon, a shift we already assigned to Cu oxidation in Figure 2c. Interestingly, oxidation is somewhat slower with Cu NCs capped with carboxylic acids than with oleylamine, yet the difference is small. Possibly, this oxidation reduction reflects the higher ligand surface concentration of carboxylic acid cappings, which may render the Cu surface less accessible to oxygen. Even so, the rapid shift of the surface plasmon in both cases indicates that neither an $OlNH_2$ nor a carboxylate ligand shell effectively protects 4 nm Cu NCs from oxidation.

To address the relation between surface ligands and sintering behavior, we cast different dispersions of Cu NCs on glass substrates and monitored the x-ray diffraction pattern of the films thus formed during sintering under inert or reductive atmospheres. Figure 6b represents the outcome of such a measurement on UDA-capped Cu NCs sintered under $N_2$. At temperatures below 200°, the diffractogram is dominated by a diffraction peak centered at 36.4°, which is characteristic of the (111) planes of $Cu_2O$. Hence, in line with the results shown in Figure 6a, we find that air exposure of the dropcast films lead to the oxidation of the initial Cu NCs. In the temperature range between 200 and 300°, the diffraction signatures of $Cu_2O$ give way for two diffraction peaks at around 43.3°and 50.4°, which correspond to the (111) and (200) planes of Cu. Hence, mild thermal sintering suffices to reduce $Cu_2O$ NCs and form metallic Cu.

Comparing sintering of Cu NCs with three different carboxylic acid ligands under $N_2$, we find that more volatile ligands give rise to somewhat lower transition temperatures, from ∼280°in the case of oleic acid to ∼260°in the case of MEEAA (see Figure 6c). The same trend appears during sintering under reductive $N_2$ : $H_2$ mixtures, where MEEAA-capped $Cu_2O$ NCs reduce to form Cu at a transition temperature of only ∼240°. While the difference in sintering temperature upon changing ligands is modest, sintering leads to significantly larger crystallites in the case of MEEAA ligands. Analysing, for example, the various diffractograms recorded at 300°by means of the DebyeScherrer equation, we estimate that sintering oleic acid or UDA capped $Cu_2O$ NCs under a reductive atmosphere results

in a grain size of ∼9 and ∼14 nm, respectively. In the case of MEEAA-capped NCs, on the other hand, we obtain a grain size close to 50 nm. Possibly, this difference is related to MEEAA being the only assessed ligand with a boiling point lower than the transition temperature. This implies that sintering occurs in a layer from which most of the organic fraction has evaporated; an aspect that seems to have clear benefits for sintering.

# 4 Discussion

Understanding the ligand-surface interaction remains a key question for metal NC research.[28] In the case of semiconductor and metal oxide NCs, significant progress resulted from the introduction of the covalent bond classification to describe ligand binding motifs.[19,29] Here, ligands are classified as L, X or Z depending on the number of electrons the equivalent neutral compound contributes to the ligand-NC bond. In this respect, L-type and Z-type ligands are Lewis bases and Lewis acids, that contribute 2 electrons or take two electrons to form the ligand-NC bond, respectively. X-type ligands, on the other hand, are radicals that form a two-electron bond with a NC by bringing in one electron and taking one electron from a NC surface atoms. In practice, this makes X-type ligands often appear as cations or anions, such as aliphatic carboxylates, phosphonates or thiolates.

Since the entire NC-ligand object must be charge neutral in apolar dispersions,[30,31] the negative charge acquired by the X-type ligands is compensated by an excess of metal cations in the case of NCs of binary compounds such as CdSe, PbS or InP.[32–34] A different behavior was reported for metal oxide NCs such as $HfO_2$. Here, it was found that the binding of a carboxylate was accompanied by the adsorption of a proton at the NC surface, forming a neutral pair of X-type ligands.[35] In a rare study on binding of secondary phosphine oxide X-type ligands ($R_1R_1PO^\bullet$) to gold NCs on the other hand, it was demonstrated that charge neutrality was ensured by the formation of $Au^{1+}$ surface atoms.[36]

A key difference between the binding of a pair of X-type ligands and a single X-type

ligand is the exchange behavior with respect to an L-type ligand such as an alkylamine. The need to preserve charge neutrality prevents such a direct exchange in the case that single X-type ligands are bound to metal-rich binary compounds or, for one thing, partially oxidized pure compounds. As a result, exposure of CdSe or PbS to alkylamines leads to the displacement of entire metal carboxylate moieties.[37] A pair of X-type ligands, on the other hand, can associate to form a neutral moiety that can be exchanged for or displaced by a neutral L-type ligand.[20] Such differences make ligand titrations a sensitive probe to understand the binding motif of ligands to a NC surface.

Here, we found that titrating $OlNH_2$ passivated Cu NCs with a carboxylic acid like undecenoic acid (UDA) induces the direct exchange of $OlNH_2$ for UDA. Moreover, FTIR spectroscopy indicates that the bound UDA is a carboxylate rather than a carboxylic acid. Both observations point towards the dissociation of UDA into undecenoate and a proton upon binding to Cu NCs to form a pair of X-type ligands that is exchangeable for $OlNH_2$. For such a dissociation to take place, an amphoteric surface is needed that provides both acidic and basic adsorption sites. Unlike the surface of a pure metal such as Cu, such distinct binding sites are a common characteristic of metal oxide surfaces.[38] This indicates that the dissociative binding of UDA to Cu NCs involves binding sites related to surface oxides, rather than the pristine Cu surface. A second result of the UDA titration of $OlNH_2$ passivated Cu NCs was the initially quantitative replacement of $OlNH_2$ by UDA. As outlined in Supporting Information S5, such a behavior is characteristic of two ligands competing for the same binding site.

Figure 7 summarizes the conclusions of the above discussions in a surface chemistry model of Cu NCs. As synthesized Cu NCs have a capping consisting of tightly bound $OlNH_2$ that interacts as an L-type ligand with acidic surface sites, which we interpret as surface-bound $Cu^{1+}$. This result is not unlikely. While alkylamines are weak, dynamic ligands for binary compounds such as CdSe and PbS,[18] octadecyalamine and oleylamine were shown to bind tightly to $Cu^{1+}$ compounds such as $CuInS_2$.[39] As outlined in Figure 7, exposure of $OlNH_2$-

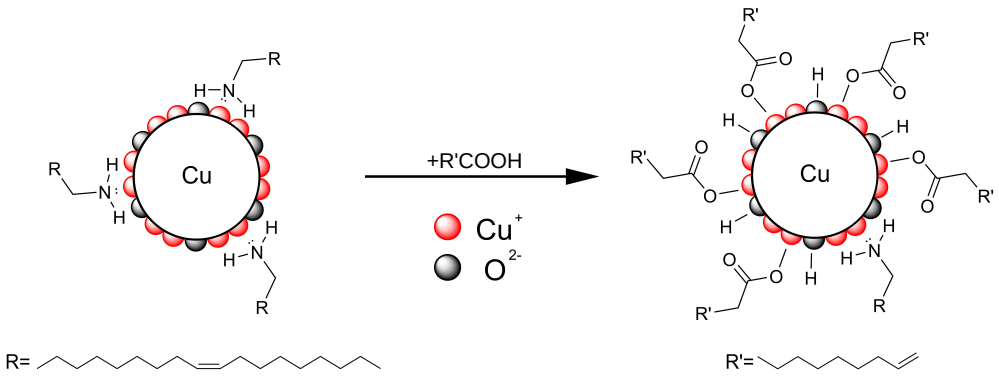


Figure 7: Surface chemistry model of the Cu NCs before and after addition of a carboxylic acid. The binding of the carboxylate to the metal is indicative and not meant to represent a specific binding mode.

capped Cu NCs to UDA results in the replacement of $OlNH_2$ by dissociated UDA at these copper oxide surface sites. This outcome agrees with previous studies on ligand binding to $Cu_2O$, where it was shown that the interaction of oleic acid with $Cu_2O$ leads to the formation of strongly bound oleate.[40] Finally, the surface chemistry model represented in Figure 7 also includes the addition of UDA to unoccupied copper oxide sites, a process that accounts for the observed increase in ligand surface concentration upon UDA exposure. This latter point suggests that, in line with recent studies on CdSe NCs,[41–43] Cu NCs offer a heterogeneous set of binding sites, where some have little affinity for $OlNH_2$ while still binding UDA. This miscellaneous surface composition is alleged to origin in the polydispersity of the NCs size distribution that provides a set of facets where organic ligands can bind with different affinities.[44]

As most metals are prone to oxidation, controlling the concentration of oxides at the surface of a metal NCs such as Cu is difficult. In a recent study, for example, Cure *et al.* reported that even if alkylamines can strongly suppress the full oxidation of copper NC, initial surface oxidation occurs rapidly.[45] The finding that the surface chemistry of Cu NCs depends on the presence of surface oxides therefore implies that the surface concentration of ligands and the occurrence or not of ligand exchange reactions can strongly depend on synthesis and processing conditions. This conclusion highlights the case for in-depth surface chemistry

studies, where surface termination by ligands is studied as a function of the composition of the NC surface as exemplified by recent work on silver NCs.[46]

# 5 Conclusion

We have demonstrated that the decomposition of copper formate in oleylamine results in $\sim 4$ nm copper nanocrystals (NCs) capped by oleylamine ($OlNH_2$). Taking such as-synthesized copper nanocolloids as a starting point, we investigated the binding of different ligands to copper nanocrystals. Using solution NMR spectroscopy, we showed that the initial $OlNH_2$ ligands can be replaced through mass action by carboxylic acids. Based on the thermodynamic description of the amine/carboxylic acid titration curves, we argue that carboxylic acids directly replace $OlNH_2$ and bind to additional surface sites that show little affinity for $OlNH_2$. Interestingly, we demonstrate that carboxylic acids dissociate upon binding, forming an $X_2$ binding motif. Since such a binding motif requires an amphoteric surface that offers acidic and basic binding sites, we argue that ligand binding to Cu nanocrystals is determined by the presence of surface oxides, rather than by the properties of the pristine metal surface. Finally, we make use of these insights in surface termination to prepare stable copper nanocolloids in a variety of polar solvents by replacing $OlNH_2$ by 2-[2-(2-methoxyethoxy)ethoxy]acetic acid and we show that the inevitable oxidation of these small NCs can be readily undone by mild thermal annealing. In this way, we turn an as-synthesized, apolar copper nanocolloid into an ink that can be formulated to produce metallic copper strips by screen or inkjet printing; a key step to use copper nanocrystals for printed electronics.

# Acknowledgement

Z.H. acknowledges SIM-Flanders (ICON-Met@link) and Ghent University (GOA 01G01513) for funding. JDR thanks Ghent University for funding.

## Supporting Information Available

The Supporting Information provides (1) the assignment of NMR resonance of oleylamine (S1), undecenoic acid (S4), and 2-[2-(2-methoxyethoxy)ethoxy]acetic acid (S8), (2) a reference $^{1}$H NMR spectrum recorded on CdSe nanocrystals (S2), (3) a DOSY analysis of a dispersion of oxidized Cu nanocrystals (S3), and (4) an overview of the different thermodynamic models used to describe the $OlNH_2$/UDA titration (S5, S6, and S7).

## References


(1) Xu, Q.; Zhao, Y.; Xu, J. Z.; Zhu, J. J. Preparation of Functionalized Copper Nanoparticles and Fabrication of a Glucose Sensor. *Sensor. Actuat. B-Chem.* **2006**, *114*, 379–386.

(2) Lee, S.; Choi, S. U. S.; Li, S.; Eastman, J. A. Measuring Thermal Conductivity of Fluids Containing Oxide Nanoparticles. *J. Heat Transf.* **1999**, *121*, 280–289.

(3) Darugar, Q.; Qian, W.; El-Sayed, M.; Pileni, M. Size-Dependent Ultrafast Electronic Energy Relaxation and Enhanced Fluorescence of Copper Nanoparticles. *J. Phys. Chem. B* **2006**, *110*, 143–149.

(4) Wang, Z.; Chen, B.; Rogach, A. L. Synthesis, Optical Properties and Applications of Light-Emitting Copper Nanoclusters. *Nanoscale Horiz.* **2017**, *2*, 135–146.

(5) Wang, Y.; Asefa, T. Poly(allylamine)-Stabilized Colloidal Copper Nanoparticles: Synthesis, Morphology, and Their Surface-Enhanced Raman Scattering Properties. *Langmuir* **2010**, *26*, 7469–7474.

(6) Ramani, T.; Leon Prasanth, K.; Sreedhar, B. Air Stable Colloidal Copper Nanoparticles: Synthesis, Characterization and their Surface-Enhanced Raman Scattering Properties. *Physica E* **2016**, *77*, 65–71.

(7) Zhang, P.; Sui, Y.; Wang, C.; Wang, Y.; Cui, G.; Wang, C.; Liu, B.; Zou, B. A One-Step Green Route to Synthesize Copper Nanocrystals and their Applications in Catalysis and Surface Enhanced Raman Scattering. *Nanoscale* **2014**, 5343–5350.

(8) Dang, R.; Song, L.; Dong, W.; Li, C.; Zhang, X.; Wang, G.; Chen, X. Synthesis and Self-Assembly of Large-Area Cu Nanosheets and their Application as an Aqueous Conductive Ink on Flexible Electronics. *ACS Appl. Mater. Inter.* **2014**, *6*, 622–629.

(9) Kang, J. S.; Kim, H. S.; Ryu, J.; Thomas Hahn, H.; Jang, S.; Joung, J. W. Inkjet Printed Electronics Using Copper Nanoparticle Ink. *J. Mater. Sci. Mater. El.* **2010**, *21*, 1213–1220.

(10) Kamyshny, A.; Magdassi, S. Conductive Nanomaterials for Printed Electronics. *Small* **2014**, 3515–3535.

(11) Rice, D. W. Atmospheric Corrosion of Copper and Silver. *J. Electrochem. Soc.* **1981**, *128*, 275.

(12) Ziegler, K. J.; Doty, R. C.; Johnston, K. P.; Korgel, B. A. Synthesis of Organic Monolayer-Stabilized Copper Nanocrystals in Supercritical Water. *J. Am. Chem. Soc.* **2001**, *123*, 7797–7803.

(13) Kanninen, P.; Johans, C.; Merta, J.; Kontturi, K. Influence of Ligand Structure on the Stability and Oxidation of Copper Nanoparticles. *J. Colloid Interf. Sci.* **2008**, *318*, 88–95.

(14) Glaria, A.; Cure, J.; Piettre, K.; Coppel, Y.; Turrin, C.-O.; Chaudret, B.; Fau, P. Deciphering Ligands' Interaction with Cu and Cu2O Nanocrystal Surfaces by NMR Solution Tools. *Chemistry* **2015**, *21*, 1169–78.

(15) Shi, M.; Kwon, H. S.; Peng, Z.; Elder, A.; Yang, H. Effects of Surface Chemistry on the

Generation of Reactive Oxygen Species by Copper Nanoparticles. *ACS Nano* **2012**, *6*, 2157–2164.

(16) Finšgar, M.; Milošev, I. Inhibition of Copper Corrosion by 1,2,3-Benzotriazole: A Review. *Corros. Sci.* **2010**, *52*, 2737–2749.

(17) Smith, A. M.; Johnston, K. A.; Crawford, S. E.; Marbella, L. E.; Millstone, J. E. Ligand Density Quantification on Colloidal Inorganic Nanoparticles. *Analyst* **2017**, *142*, 11–29.

(18) Hens, Z.; Martins, J. C. A Solution NMR Toolbox for Characterizing the Surface Chemistry of Colloidal Nanocrystals. *Chem. Mater.* **2013**, *25*, 1211–1221.

(19) De Roo, J.; De Keukeleere, K.; Hens, Z.; Van Driessche, I. From Ligands to Binding Motifs and Beyond; the Enhanced Versatility of Nanocrystal Surfaces. *Dalt. Trans.* **2016**, *45*, 13277–13283.

(20) De Roo, J.; Justo, Y.; De Keukeleere, K.; Van den Broeck, F.; Martins, J. C.; Van Driessche, I.; Hens, Z. Carboxylic-Acid-Passivated Metal Oxide Nanocrystals: Ligand Exchange Characteristics of a New Binding Motif. *Ang. Chem. Int. Ed.* **2015**, *54*, 6488–6491.

(21) De Roo, J.; Yazdani, N.; Drijvers, E.; Lauria, A.; Maes, J.; Owen, J. S.; Van Driessche, I.; Niederberger, M.; Wood, V.; Martins, J. C. et al. Probing SolventLigand Interactions in Colloidal Nanocrystals by the NMR Line Broadening. *Chem. Mater.* **2018**, *30*, 5485–5492.

(22) Sun, X.; Zhang, Y.-W.; Si, R.; Yan, C.-H. Metal (Mn, Co, and Cu) Oxide Nanocrystals from Simple Formate Precursors. *Small* **2005**, *1*, 1081–1086.

(23) Brenner, A.; Harris, E. A Quantitative Test for Copper Using Bicinchoninic Acid. *Anal. Biochem.* **1995**, *226*, 80–84.

(24) Johnson, P. B.; Christy, R. W. Optical Constants of the Noble Metals. *Phys. Rev. B* **1972**, *6*, 4370–4379.

(25) Hens, Z.; Moreels, I. Light Absorption by Colloidal Semiconductor Quantum Dots. *J. Mater. Chem.* **2012**, *22*, 10406.

(26) Singh, M.; Sinha, I.; Premkumar, M.; Singh, A.; Mandal, R. Structural and Surface Plasmon Behavior of Cu Nanoparticles Using Different Stabilizers. *Colloids Surfaces A Physicochem. Eng. Asp.* **2010**, *359*, 88–94.

(27) Khutsishvili, S. S.; Vakulskaya, T. I.; Kuznetsova, N. P.; Ermakova, T. G.; Pozdnyakov, A. S.; Prozorova, G. F. Formation of Stable Paramagnetic Nanocomposites Containing Zero-Valence Silver and Copper in a Polymeric Matrix. *J. Phys. Chem. C* **2014**, *118*, 19338–19344.

(28) Jin, R.; Zeng, C.; Zhou, M.; Chen, Y. Atomically Precise Colloidal Metal Nanoclusters and Nanoparticles: Fundamentals and Opportunities. *Chem. Rev.* **2016**, *116*, 10346–10413.

(29) Owen, J. The Coordination Chemistry of Nanocrystal Surfaces. *Science* **2015**, *347*, 615–616.

(30) Shim, M.; Guyot-Sionnest, P. Permanent Dipole Moment and Charges in Colloidal Semiconductor Quantum Dots. *J. Chem. Phys.* **1999**, *111*, 6955–6964.

(31) Cirillo, M.; Strubbe, F.; Neyts, K.; Hens, Z. Thermal Charging of Colloidal Quantum Dots in Apolar Solvents: A Current Transient Analysis. *ACS Nano* **2011**, *5*, 1345–1352.

(32) Voznyy, O. Mobile surface traps in CdSe nanocrystals with carboxylic acid ligands. *J. Phys. Chem. C* **2011**, *115*, 15927–15932.

(33) Cros-Gagneux, A.; Delpech, F.; Nayral, C.; Cornejo, A.; Coppel, Y.; Chaudret, B.

Surface Chemistry of InP Quantum Dots: A Comprehensive Study. *J. Am. Chem. Soc.* **2010**, *132*, 18147–18157.

(34) Moreels, I.; Justo, Y.; De Geyter, B.; Haustraete, K.; Martins, J. C.; Hens, Z. Size-Tunable, Bright, and Stable PbS Quantum Dots: A Surface Chemistry Study. *ACS Nano* **2011**, *5*, 2004–2012.

(35) De Roo, J.; Van Den Broeck, F.; De Keukeleere, K.; Martins, J. C.; Van Driessche, I.; Hens, Z. Unravelling the Surface Chemistry of Metal Oxide Nanocrystals, the Role of Acids and Bases. *J. Am. Chem. Soc.* **2014**, *136*, 9650–9657.

(36) Cano, I.; Huertos, M. A.; Chapman, A. M.; Buntkowsky, G.; Gutmann, T.; Groszewicz, P. B.; van Leeuwen, P. W. N. M. Air-Stable Gold Nanoparticles Ligated by Secondary Phosphine Oxides as Catalyst for the Chemoselective Hydrogenation of Substituted Aldehydes: a Remarkable Ligand Effect. *J. Am. Chem. Soc.* **2015**, *137*, 7718–7727.

(37) Anderson, N. C.; Hendricks, M. P.; Choi, J. J.; Owen, J. S. Ligand Exchange and the Stoichiometry of Metal Chalcogenide Nanocrystals: Spectroscopic Observation of Facile Metal-Carboxylate Displacement and Binding. *J. Am. Chem. Soc.* **2013**, *135*, 18536–18548.

(38) Blesa, M.; Weisz, A.; Morando, P.; Salfity, J.; Magaz, G.; Regazzoni, A. The Interaction of Metal Oxide Surfaces with Complexing Agents Dissolved in Water. *Coordin. Chem. Rev.* **2000**, *196*, 31–63.

(39) Dierick, R.; Van den Broeck, F.; De Nolf, K.; Zhao, Q.; Vantomme, A.; Martins, J. C.; Hens, Z. Surface Chemistry of $CuInS_2$ Colloidal Nanocrystals, Tight Binding of L-Type Ligands. *Chem. Mater.* **2014**, *26*, 5950–5957.

(40) Kauffman, D. R.; Ohodnicki, P. R.; Kail, B. W.; Matranga, C. Selective Electrocatalytic

Activity of Ligand Stabilized Copper Oxide Nanoparticles. *J. Phys. Chem. Lett.* **2011**, *2*, 2038–2043.

(41) Aruda, K. O.; Amin, V. A.; Thompson, C. M.; Lau, B.; Nepomnyashchii, A. B.; Weiss, E. A. Description of the Adsorption and Exciton Delocalizing Properties of p-Substituted Thiophenols on CdSe Quantum Dots. *Langmuir* **2016**, *32*, 3354–3364.

(42) Drijvers, E.; De Roo, J.; Martins, J. C.; Infante, I.; Hens, Z. Ligand Displacement Exposes Binding Site Heterogeneity on CdSe Nanocrystal Surfaces. *Chem. Mater.* **2018**, *30*, 1178–1186.

(43) Saniepay, M.; Mi, C.; Liu, Z.; Abel, E. P.; Beaulac, R. Insights into the Structural Complexity of Colloidal CdSe Nanocrystal Surfaces: Correlating the Efficiency of Non-radiative Excited-State Processes to Specific Defects. *J. Am. Chem. Soc.* **2018**, *140*, 1725–1736.

(44) Puzder, A.; Williamson, A. J.; Zaitseva, N.; Galli, G.; Manna, L.; Alivisatos, A. P. The Effect of Organic Ligand Binding on the Growth of CdSe Nanoparticles Probed by *Ab Initio* Calculations. *Nano Lett.* **2004**, *4*, 2361–2365.

(45) Cure, J.; Glaria, A.; Collière, V.; Fazzini, P. F.; Mlayah, A.; Chaudret, B.; Fau, P. Remarkable Decrease in the Oxidation Rate of Cu Nanocrystals Controlled by Alkylamine Ligands. *J. Phys. Chem. C* **2017**, *121*, 5253–5260.

(46) Johnston, K. A.; Smith, A. M.; Marbella, L. E.; Millstone, J. E. Impact of As-Synthesized Ligands and Low-Oxygen Conditions on Silver Nanoparticle Surface Functionalization. *Langmuir* **2016**, *32*, 3820–3826.

# Graphical TOC Entry